Received: 21 April 2022 | Revised: 13 September 2022 | Accepted: 26 October 2022

DOI: 10.1002/nme.7158

RESEARCH ARTICLE

WILEY

On non-parametric fatigue optimization

Roman Sartorti[1] | **Torsten Möcker**[2] | **Benedikt Kriegesmann**[1] | **Claus B.W. Pedersen**[2]

[1]Institute for Structural Mechanics in Lightweight Design, Hamburg University of Technology, Hamburg, Germany

[2]Dassault Systèmes Deutschland GmbH, Hamburg, Germany

Correspondence
Roman Sartorti, Institute for Structural Mechanics in Lightweight, Eißendorfer Straße 40, 21073 Hamburg, Germany.
Email: roman.sartorti@tuhh.de

Abstract

The present work presents a novel approach for semi-analytic adjoint sensitivity-based design optimization for nonproportional fatigue damage. In order to apply fatigue damage in sensitivity-based design optimizations, an essential part is to calculate correct sensitivities. However, this is not straight forward since fatigue damage calculation typically include rainflow counting and critical plane search algorithms. Therefore, no derivatives are directly available for the fatigue damage calculation, only functional values given by numerical computation. In existing literature the considered fatigue damage calculation is simplified until a closed-form differentiability is satisfied. However, these simplifications are not applicable for industrial examples where accurate fatigue life estimates are required. In the present work numerical differentiation of the fatigue damage values with respect to the stress tensor is applied to calculate semi-analytical adjoint sensitivities at material points for multiple load cases. The proposed method is verified and demonstrated using different damage parameter types including critical plane analysis. Additionally, different academic and industrial numerical examples are compared to stress and stiffness optimized designs. The fatigue damage optimized designs show improved fatigue damage results for both the specific damage parameter types and when comparing to stress and stiffness optimized designs. Furthermore, it is successfully applied for different design variables (sizing, non-parametric shape and bead) as well as different optimization formulations using fatigue damage either as objective or constraint.

KEYWORDS

critical planes, damage parameters, fatigue damage, non-parametric optimization, rainflow counting, semi-analytical adjoint sensitivities

1 | INTRODUCTION

Sensitivity-based design optimization methods are widely used to find the optimal design regarding a given objective and given constraints. Typical objectives are compliance minimizing subject to a volume constraint or volume minimizing

[Correction added on 03 December 2022, after first online publication: The term "nonparametric" throughout the paper has been corrected to "non-parametric" in this current version.]

subject to strength constraints. Those strength constraints are usually considered for static load cases. However, a structural part is often exited with time dependent loads. Those time-dependent loadings lead to fatigue damage in the structure where the location does not necessarily match the static failure location. Therefore, it is also important to include fatigue damage to ensure that a structural part is resistant against fatigue failure.

The required sensitivity calculation of fatigue damage is numerically challenging as high-cycle fatigue (HCF) damage analysis in practice has several discontinuous modelling characteristics. Normally, considering static criterion for fatigue failure is not sufficient as loads change over time, that is, have certain time histories. The load variations in time lead to HCF damage failure by the initiation of micro cracks in the material.[1-5] Especially, when encountering multiaxial loading fatigue failure frequently appears at locations different from those predicted by the static analyses as shown in Figure 1. Thus, considering advanced fatigue damage criteria that account for multiaxial stress variant loading is essential for obtaining reliable optimized designs.

Many publications on fatigue optimization consider topology optimization design variables. Holmberg[6,7] considers fatigue calculations decoupled from the optimizations by converting the fatigue constraints into stress constraints. Initially, an optimization is performed to find the maximum allowable stress yielding the fatigue constraint for a given proportional load history. Then the first principal stress criterion is considered as stress constraint in a stress-based optimization.

Fatigue damage is directly included in the optimization framework by Jeong[8] using a signed von Mises criterion for a stress-life approach. The stresses are calculated for static and harmonic finite element procedures. Here one key aspect is that the nondifferentiability of the mean stress corrections (MSCs) is replaced by smooth approximations under constant and proportional mechanical loads. Oest and Lund[9] and Olesen et al.[10] address a more general optimization method

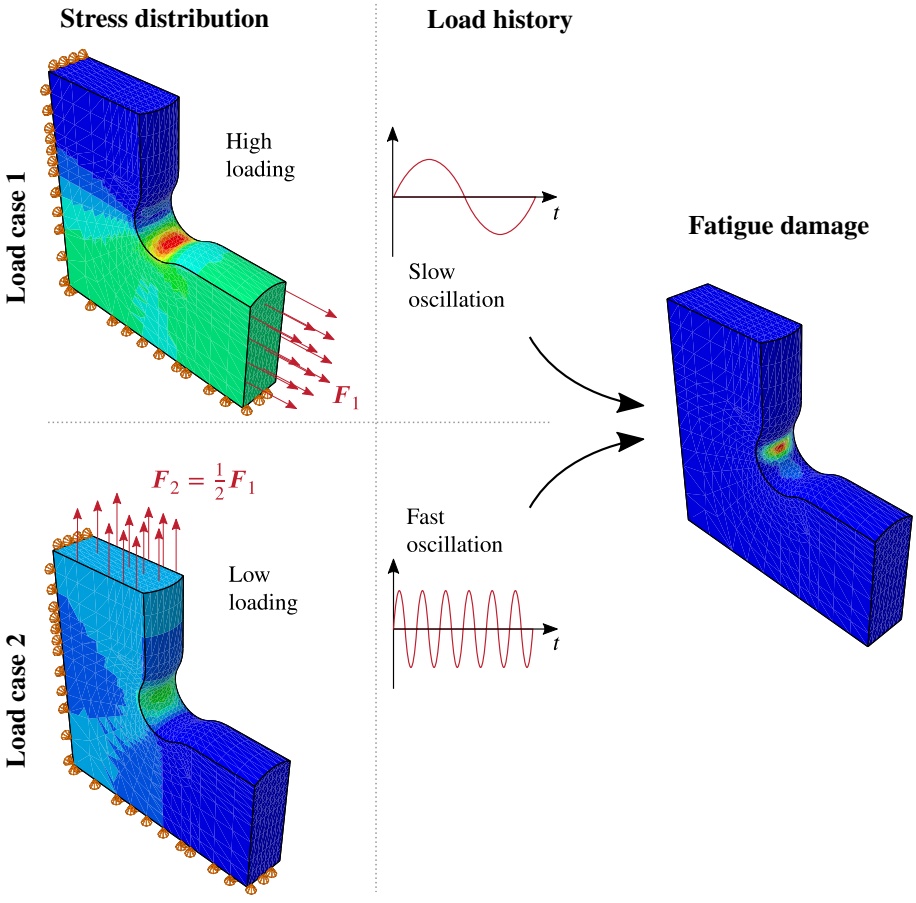

FIGURE 1 Contour plots for stress and fatigue damage distribution. The first load case leads to the highest von Mises stress, that is, being the most critical load case for static strength. However, due to the slow oscillation of load case one, then the second load case is more critical for fatigue damage. As visible, the fatigue damage hotspot does not correspond to the stress hotspot. Thus, minimizing maximum stress is not equal to minimizing maximum fatigue damage.

for fatigue damage optimization including rainflow counting for the load time histories. The rainflow counting for the proportional loading is performed using the load history because the stresses scale linearly with respect to the input load. A stress-life relationship is applied and the Sines damage parameter is considered in Oest.[9] A recent publication by Olesen[10] studies the principal stress as damage parameter for the fatigue calculation for a transversely isotropic material. Furthermore, Zhang[11] proposes a method incorporating more realistic nonproportional load scenarios considering signed von Mises as damage parameter and rainflow counting of the stress history. This leads to higher computational costs since rainflow counting is performed for every material point. To avoid rainflow counting Suresh[12,13] proposes a continuous damage accumulation approach in time which also supports nonproportional loading. However, this causes significant computational costs as the time histories are calculated explicitly while having long time histories.

As previously mentioned, most publications consider topology optimization. However, a few publications address different design variables such as sizing thickness and diameter of circular beams for sensitivity based fatigue damage optimization. Oest[14,15] shows the sizing optimization of jacket structures for offshore wind turbines considering the thickness and diameter of circular finite element beams. As Oest[14,15] does not include MSCs for the fatigue damage calculation and the damage parameter is formulated using wind turbine certification rules without critical plane analysis for fatigue damage calculation.

In Reference 16, sizing thickness optimization of weld lines for shell structures is performed based upon a fatigue damage calculation formulated in forces instead of stresses and contains no critical plane analysis.

All above-mentioned literature and references therein have in common that they are limited to very specific use cases of fatigue damage modeling. Typically, the fatigue damage modeling is simplified significantly so that one obtains analytically differentiable closed-form equations, for example, by using damage parameter types that are directly differentiable such as von Mises stress, principal stress etc. Frequently, only proportional loading is incorporated to reduce the computational effort and to avoid critical plane analysis, which so far has never been considered in sensitivity-based optimization. Critical plane analysis is common practice in industry for regular metals subject to non-proportional load conditions requiring sign dependent (tension versus compression) damage parameter types as such as Brown-Miller, Normal Stress or Normal Strain. Thus, these previously mentioned simplifications lead to fatigue damage modeling formulations that do not provide accurate fatigue life predictions and, hence, are less relevant for practical applications. Moreover, the proposed methods are often restricted to specific design variable types. In contrast, the present work derives an adaptable semi-analytically adjoint sensitivity-based design optimization approach for numerous design variables and damage parameter types including rainflow counting, MSC, multiple load cases, nonproportional loading and critical plane analysis which to the author's knowledge has not been proposed previously.

The paper is organized as follows. Section 2 summarizes the theory and methodology for HCF damage analysis. The formulation for fatigue damage optimization is defined in Section 3.1 followed by a definition of design variables in Section 3.2. Afterwards, the derivation of semi-analytical adjoint sensitivities are derived in Section 3.3. Section 4 describes the numerical implementation verified using the results of finite difference calculations that are compared to both the partial fatigue damage derivatives with respect to the stress tensor and the fatigue damage sensitivities with respect to the design variables. Section 5 shows three numerical examples verifying that the optimization approach is able to address common modeling practice for HCF damage as well as different damage parameter types and various design variable types. General conclusions and numerical observations are summarized in Section 6.

2 | THEORY

2.1 | Structural equilibrium

The structural behavior is analyzed using the linear finite element method.[17] All examples are considered to be quasi-static and without nonlinearities. Thus, the whole system is described by the linear system of equations

$$\boldsymbol{K}\boldsymbol{u}^{(\ell)} = \boldsymbol{P}^{(\ell)}. \tag{1}$$

where $\boldsymbol{K}$ is the stiffness matrix, $\boldsymbol{u}^{(\ell)}$ are the displacements, and $\boldsymbol{P}^{(\ell)}$ describes the external loads for all load cases $\ell = 1, \dots, L$. Since the system is linear, the stiffness matrix has to be factorized only once for all load cases improving computational performance.

In order to perform fatigue damage analysis the stress tensors $\sigma_{ij_k}^{(\ell)}$ are required for each load case ℓ and at each material point k. Those are derived using the strain displacement matrix $\mathbf{B}$ and the constitutive material matrix $\mathbb{C}$. Thus, the stress tensor $\sigma_{ij_k}^{(\ell)}$ at each material point k for load case ℓ is calculated by applying

$$\sigma_{ij_k}^{(\ell)} = \mathbb{C}\mathbf{B}\boldsymbol{u}_k^{(\ell)}, \tag{2}$$

where $\boldsymbol{u}_k^{(\ell)}$ is the displacement of material point k.

2.2 | Fatigue damage calculation

This section does not aim at giving a detailed description of fatigue damage calculation but intends to describe the most important aspects for the present work as well as the requirements for deriving semi-analytical adjoint sensitivities. For more details on fatigue damage analysis see References 5,18,19 and references therein.

2.2.1 | Material properties

In order to calculate the maximum number of cycles to failure N_f a stress-life (SN) or strain-life relation is required. For stress-based methods SN curves are either defined by discrete data points being linearly interpolated or using a conventional SN relation, that is, using Basquin's equation. The stress amplitude σ_a is related to the number of cycles to failure N_f having an exponential law where b is the Basquin's factor and σ_f' is the fatigue strength yielding

$$\sigma_\mathrm{a} = \sigma_\mathrm{f}'(2N_\mathrm{f})^b. \tag{3}$$

Stress-based methods are typically used for HCF while strain-based methods are applied for both, HCF and low-cycle fatigue (LCF). Strain-based methods have an additional term representing the observation that strains are the damage driver for LCF. Therefore, additionally the fatigue ductility ε_f' as well as the Coffin–Manson exponent c are required to describe the maximum strain amplitude ε_a. The strain-life (EN) curve is described with

$$\varepsilon_\mathrm{a} = \frac{\sigma_\mathrm{f}'}{E}(2N_\mathrm{f})^b + \varepsilon_\mathrm{f}'(2N_\mathrm{f})^c, \tag{4}$$

where E is the Young's modulus of the material. For HCF the fatigue damage solvers typically take only stresses as input values, that is, strains need to be derived from stresses. Therefore, the Poisson's ratio ν is needed for damage calculation.

Typical EN- and SN-curves are presented in Figure 2. The EN-curve visualizes the contributions of both parts contributing to the strain-life. As shown, the strain part is dominant for low cycle numbers while the stresses dominate for high cycle regions. Further details are discussed in Lee.[5] In this paper we consider only HCF. Otherwise plastic strains or approximated plastic strains are required for the fatigue calculation.

2.2.2 | Fatigue calculation workflow

A representative standard workflow of fatigue damage calculation is shown in Figure 3. First, the stresses from a Finite Element Analysis (FEA) of all required load cases are imported. Each load case has its own prescribed load history $g^{(\ell)}(t)$. Then the stresses in time are calculated by linear superposition using the time histories of the multiple load cases as the following:

$$\sigma_{ij_k}(t) = \sum_{\ell=1}^{L} \sigma_{ij_k}^{(\ell)} g^{(\ell)}(t). \tag{5}$$

The loading is referred to as proportional if there is only one load case and for multiple load cases as *nonproportional*.

Afterwards an appropriate damage parameter is selected. Typically, the choice of a damage parameter depends on the considered material. Besides, the life range is important, that is, if a HCF or a LCF problem is to be analyzed. While stress based methods are only accurate for HCF, strain-based methods are applicable to both HCF and LCF. Most

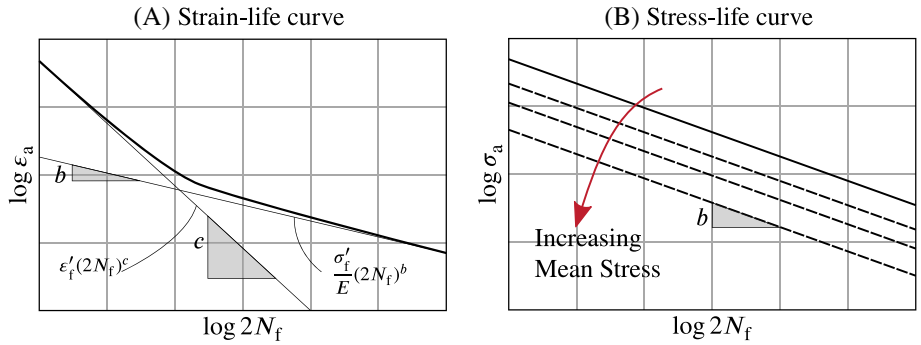

FIGURE 2 (A) Strain-life curve being a superposition of a plastic strain part dominant for low-cycle fatigue and an elastic strain part dominant for high-cycle fatigue. As indicated, in the double logarithmic plot the material parameters b and c describe the slope of the curve. (B) Stress-life curve showing the influence of mean stresses on fatigue life. Typically, higher mean stresses reduce the maximum number of cycles to failure, that is, increase the predicted fatigue damage.

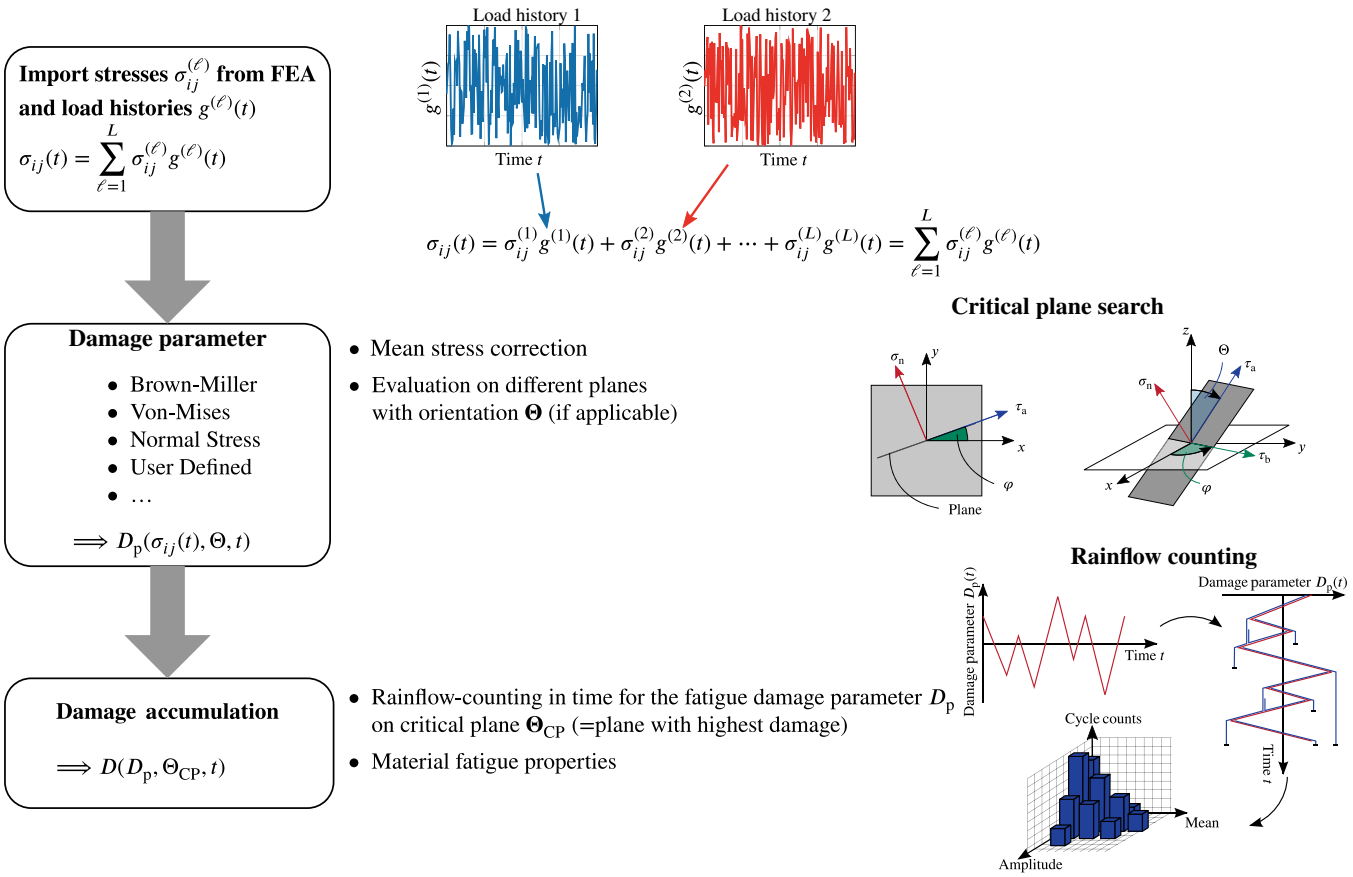

FIGURE 3 Fatigue damage calculation workflow. Initially, the stresses from finite element analysis for L load cases and the corresponding load histories are combined by linear superposition in time. Secondly, the time history of the damage parameter is calculated taking mean stress corrections into account. For damage parameters depending on directional stresses the critical plane method is applied. Lastly, damage accumulation is performed by means of rainflow counting. The plane having the largest damage value is chosen as the critical plane.

accurate fatigue results for ductile materials are often obtained using the strain based Brown–Miller damage parameter. The Brown–Miller fatigue damage parameter is originally suggested by Brown and Miller.[20] Later a slightly modified Brown–Miller damage parameter type is suggested[21,22] which is considered less conservative than the original damage parameter by Brown and Miller[20] but judged to be more accurate. Hence, the Brown–Miller damage parameter defined in References 21,22 is applied in the present work. Again, we emphasize that the various versions of the Brown–Miller fatigue model are supported by the present approach for the adjoint sensitivities. Other frequently applied damage parameters are normal stress, normal strain, or von Mises stress.

In case of nonproportional loading the principal directions change over time. Therefore, all damage parameters including normal or shear stresses or strains require a so-called *critical plane search*. The paper from Meggiolaro et al.[23] describes in detail the applied critical plane strategy in the present work as we consider the present critical plane approach to be one of the most adopted by both academia and industry. Basically, this algorithm considers a finite number of plane orientations on which normal and/or shear stresses are evaluated to calculate the damage parameter time history, see References 5,24,25 for further details.

Finally, a *rainflow counting* algorithm is applied to the time history of the damage parameter in order to count similar amplitudes and mean values into different bins. The mean values are required when a MSC is considered which is normal practice. Those methods are used to account for the effect of different mean values on the fatigue life. For each bin s the maximum number of cycles to failure N_{f_s} is calculated. The accumulated damage D_k per material point k is then determined using Palmgren–Miners rule. This rule compares the counted cycles n_s per bin with the maximum number of cycles to failure N_{f_s} to calculate the amount of damage caused by the given bin. The accumulated damage is then the sum of damage contributions from all bins s where $s = 1, 2, \dots, S$:

$$D_k = \sum_{s=1}^{S} \frac{n_s}{N_{f_s}}. \tag{6}$$

3 | OPTIMIZATION

3.1 | Optimization formulation

The optimization is formulated in terms of an objective function g_0 and I constraints g_i having an upper and lower constraint value g_i^{U} and g_i^{L}, respectively. The functions g_0 and g_i are also referred to as design responses and they are generally functions of the non-parametric design variables $\boldsymbol{\varphi}$. Typically, a regularization scheme is applied to obtain physical design variables $\phi_j \in \boldsymbol{\phi}(\boldsymbol{\varphi})$ being a function of the non-parametric design variables $\boldsymbol{\varphi}$ (see Section 3.2). The design variables $\boldsymbol{\varphi}$ are typically restricted by an upper bound φ_j^{U} and a lower bound φ_j^{L} where $j = 1, 2, \dots, J$ being the number of the constrained design variable and J is the total number of constrained design variables. Moreover, the structural equilibrium has to be fulfilled for all load cases and, hence, the residual $\boldsymbol{R}^{(\ell)}$ is zero for all load cases L. Thereby, the stiffness matrix $\boldsymbol{K}$ and the displacement field $\boldsymbol{u}^{(\ell)}$ depend on the physical design variables $\boldsymbol{\phi}$. The optimization task is written as

$$\min_{\boldsymbol{\varphi}} \quad g_0(\boldsymbol{\varphi}). \tag{7}$$

$$\text{s.t.} \quad g_i^{\mathrm{L}} \le g_i(\boldsymbol{\varphi}) \le g_i^{\mathrm{U}}, \quad \text{where } i = 1, 2, \dots, I \tag{8}$$

$$\varphi_j^{\mathrm{L}} \le \varphi_j \le \varphi_j^{\mathrm{U}}, \quad \text{where } j = 1, 2, \dots, J \tag{9}$$

$$\boldsymbol{R}^{(\ell)} = \boldsymbol{K}(\boldsymbol{\phi})\boldsymbol{u}^{(\ell)}(\boldsymbol{\phi}) - \boldsymbol{P}^{(\ell)} = \boldsymbol{0} \quad \text{where } \ell = 1, 2, \dots, L. \tag{10}$$

In the present work, a sensitivity-based optimization algorithm is applied using mathematical programming. The sensitivities w.r.t the design variables $\boldsymbol{\phi}$ are calculated using the adjoint method. After introducing different design variable types and a regularization scheme, the adjoint sensitivities are derived for fatigue damage D as design response g.

3.2 | Design variables

Figure 4 shows three types of non-parametric design variables $\boldsymbol{\varphi}$ applied in the present work for Equations (7)–(10) and for which the fatigue sensitivities are derived in Section 3.3. Initially, Figure 4A shows the thickness of finite shell elements

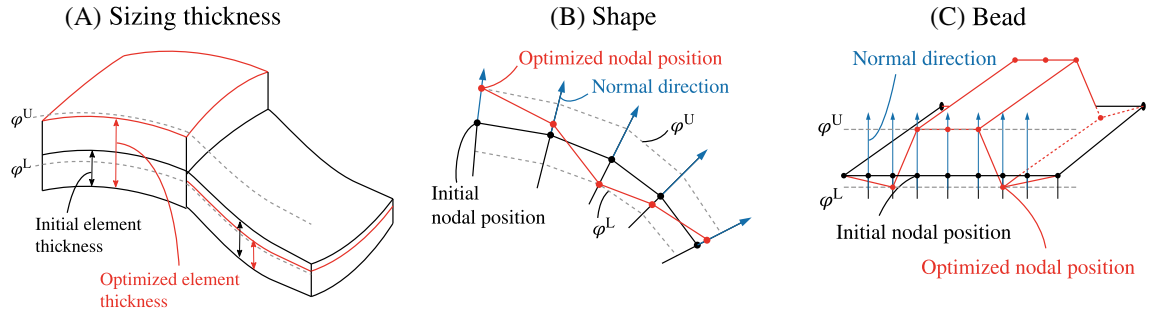

FIGURE 4 Applied non-parametric design variables. (A) Sizing thickness; (B) Shape; (C) Bead

as design variables $\boldsymbol{\varphi}$ for sizing optimization where the bounds in Equation (9) represent the lower thickness bound φ^{L} and the upper thickness bound φ^{U}, respectively. The nodal positions of finite elements are the design variables $\boldsymbol{\varphi}$ for shape optimization as shown in Figure 4B and for bead optimization as shown at Figure 4C. The nodal shape and bead design variables are moving in the normal direction of a surface consisting of continuum finite elements and shell finite elements, respectively. The movements of the nodal shape and bead design variables are constrained to the upper limit φ^{U} and the lower limit φ^{L}.

Usually, a regularization in form of filtering is present in structural optimization for introducing a length-scale so that the optimization problem is well-posed in addition to suppressing checkerboard effects or other discontinuities due to the discrete finite element idealization of a continuous continuum model, see References 26-30. For the present work, a design variable filter is applied[31,32] which defines the physical design variable ϕ_j as a weighted average of the design variables φ_m within the domain Ω_j. The domain Ω_j contains all design variables ϕ_m within a distance r_m from design variable j being smaller than the defined filter distance ρ. Thereby, the filtered design variable ϕ_j yields:

$$\phi_j = \frac{\sum_{m\in\Omega_j} w_m \varphi_m}{\sum_{t\in\Omega_s} w_m}, \tag{11}$$

where the weighting function w_m is given by the linearly decaying (cone-shape) function:[31,32]

$$w_m = \frac{\rho - r_m}{\rho}. \tag{12}$$

The sensitivity of function g in Equation (7) or (8) with respect to a change in the design variables is determined using the chain rule as

$$\frac{\partial g}{\partial \boldsymbol{\varphi}} = \frac{\partial g}{\partial \boldsymbol{\phi}} \frac{\partial \boldsymbol{\phi}}{\partial \boldsymbol{\varphi}}. \tag{13}$$

The derivative $\frac{\partial \boldsymbol{\phi}}{\partial \boldsymbol{\varphi}}$ is straightforward to compute, but the sensitivities $\frac{\partial g}{\partial \boldsymbol{\phi}}$ of the design response w.r.t. the physical design variables $\boldsymbol{\phi}$ require special attention as discussed in Section 3.3.

3.3 | Adjoint sensitivities

In structural design optimization the adjoint method is the most common approach as it allows efficient sensitivity calculation for a large number of design variables. Some background information can be found in the literature.[33-36]

For D_k being the fatigue damage at material point k, the design response depends on the stress tensor $\sigma_{ij_k}^{(\ell)}$ which depends on the physical design variables $\boldsymbol{\phi}$ and the displacements $\boldsymbol{u}^{(\ell)}(\boldsymbol{\phi})$ being also dependent on $\boldsymbol{\phi}$, that is, $D_k(\boldsymbol{\phi}, (\sigma_{ij_k}^{(\ell)}(\boldsymbol{\phi}, \boldsymbol{u}^{(\ell)}(\boldsymbol{\phi}))))$. Then all residuals $\boldsymbol{R}^{(\ell)}$ are added to the design response.

Applying the standard adjoint approach as described in the literature, only the residual for one load case is added to the given design response g. In the present approach, however, the sum of all load cases is added to the damage design

response D for deriving the adjoint system. The sum is still zero and, hence, the design response value remains unchanged. Each load case residual is multiplied with a Lagrangian multiplier $\boldsymbol{\lambda}^{(\ell)}$, also referred to as adjoint variable. Thereby, the adjoint system for D_k yields

$$D_k(\boldsymbol{\phi}, \sigma_{ij_k}^{(\ell)}(\boldsymbol{\phi}, \boldsymbol{u}^{(\ell)}(\boldsymbol{\phi}))) = D_k(\boldsymbol{\phi}, \sigma_{ij_k}^{(\ell)}(\boldsymbol{\phi}, \boldsymbol{u}^{(\ell)}(\boldsymbol{\phi}))) + \sum_{\ell=1}^{L} \boldsymbol{\lambda}^{(\ell)^\top}(\boldsymbol{K}(\boldsymbol{\phi})\boldsymbol{u}(\boldsymbol{\phi})^{(\ell)} - \boldsymbol{P}^{(\ell)}). \tag{14}$$

Differentiating D_k w.r.t. the vector of design variables $\boldsymbol{\phi}$ is then given by

$$\frac{\mathrm{d}D_k}{\mathrm{d}\boldsymbol{\phi}} = \frac{\partial D_k}{\partial \boldsymbol{\phi}} + \sum_{\ell=1}^{L}\left[\frac{\partial D_k}{\partial \sigma_{ij_k}^{(\ell)}}\frac{\partial \sigma_{ij_k}^{(\ell)}}{\partial \boldsymbol{\phi}} + \frac{\partial D_k}{\partial \sigma_{ij_k}^{(\ell)}}\frac{\partial \sigma_{ij_k}^{(\ell)}}{\partial \boldsymbol{u}^{(\ell)}}\frac{\mathrm{d}\boldsymbol{u}^{(\ell)}}{\mathrm{d}\boldsymbol{\phi}}\right] + \sum_{\ell=1}^{L}\boldsymbol{\lambda}^{(\ell)^\top}\left[\frac{\mathrm{d}\boldsymbol{K}}{\mathrm{d}\boldsymbol{\phi}}\boldsymbol{u}^{(\ell)} + \boldsymbol{K}\frac{\mathrm{d}\boldsymbol{u}^{(\ell)}}{\mathrm{d}\boldsymbol{\phi}}\right]. \tag{15}$$

$$= \frac{\partial D_k}{\partial \boldsymbol{\phi}} + \sum_{\ell=1}^{L}\left[\frac{\partial D_k}{\partial \sigma_{ij_k}^{(\ell)}}\frac{\partial \sigma_{ij_k}^{(\ell)}}{\partial \boldsymbol{\phi}} + \boldsymbol{\lambda}^{(\ell)^\top}\frac{\mathrm{d}\boldsymbol{K}}{\mathrm{d}\boldsymbol{\phi}}\boldsymbol{u}^{(\ell)}\right] + \sum_{\ell=1}^{L}\left[\frac{\partial D_k}{\partial \sigma_{ij_k}^{(\ell)}}\frac{\partial \sigma_{ij_k}^{(\ell)}}{\partial \boldsymbol{u}^{(\ell)}} + \boldsymbol{\lambda}^{(\ell)^\top}\boldsymbol{K}\right]\frac{\mathrm{d}\boldsymbol{u}^{(\ell)}}{\mathrm{d}\boldsymbol{\phi}}. \tag{16}$$

The derivatives of the displacements are eliminated for reducing numerical cost. In order to eliminate the displacement derivative $\frac{\mathrm{d}\boldsymbol{u}^{(\ell)}}{\mathrm{d}\boldsymbol{\phi}}$ the expression in the bracket in front of the derivative is set to zero for each load case. Therefore, the adjoint variables $\boldsymbol{\lambda}^{(\ell)}$ are chosen for all load cases leading to

$$\boldsymbol{0} \overset{!}{=} \frac{\partial D_k}{\partial \sigma_{ij_k}^{(\ell)}}\frac{\partial \sigma_{ij_k}^{(\ell)}}{\partial \boldsymbol{u}^{(\ell)}} + \boldsymbol{\lambda}^{(\ell)^\top}\boldsymbol{K} \text{ where } \ell = 1, 2, \ldots, L. \tag{17}$$

$$\Rightarrow \boldsymbol{K}^\top\boldsymbol{\lambda}^{(\ell)} = -\left(\frac{\partial D_k}{\partial \sigma_{ij_k}^{(\ell)}}\frac{\partial \sigma_{ij_k}^{(\ell)}}{\partial \boldsymbol{u}^{(\ell)}}\right)^\top \text{ where } \ell = 1, 2, \ldots, L. \tag{18}$$

$$\frac{\mathrm{d}D_k}{\mathrm{d}\boldsymbol{\phi}} = \frac{\partial D_k}{\partial \boldsymbol{\phi}} + \sum_{\ell=1}^{L}\left[\frac{\partial D_k}{\partial \sigma_{ij_k}^{(\ell)}}\frac{\partial \sigma_{ij_k}^{(\ell)}}{\partial \boldsymbol{\phi}} + \boldsymbol{\lambda}^{(\ell)^\top}\frac{\mathrm{d}\boldsymbol{K}}{\mathrm{d}\boldsymbol{\phi}}\boldsymbol{u}^{(\ell)}\right]. \tag{19}$$

This requires the solution of L additional adjoint systems. However, since the system is symmetric then $\boldsymbol{K}^\top = \boldsymbol{K}$ and the stiffness matrix $\boldsymbol{K}$ is already factorized from the primary solution. Thereby, the additional computational cost is mainly driven by the computation of the right hand side, also referred to as *pseudo-loads*.

Throughout this work the fatigue damage has no direct dependency on the design variables $\boldsymbol{\phi}$. Thus the partial derivative $\frac{\partial D_k}{\partial \boldsymbol{\phi}}$ is zero for all cases in the present work.

In order to apply equations (18) and (19) the sensitivities of the fatigue damage D_k need to be derived for every damage parameter. As indicated in Figure 3 there are discontinuous functions for damage calculation such as rainflow counting and critical plane search. Therefore, no analytical derivative of the fatigue damage exists. Typically, in the literature the fatigue damage calculation is simplified to not include critical plane search and/or assuming that rainflow counts remain constant and/or considering just a single damage parameter.

As mentioned then the most frequent applied industrial fatigue damage calculations include these function features in the computational workflow for the fatigue calculation and thereby, the function values are only given by the numerical computation. Therefore, no derivatives of a closed-form formulation is available for the fatigue damage calculations. The present work applies numerical differentiation for the partial fatigue damage sensitivities w.r.t. the stress tensor. These are calculated using a forward finite difference approximation as

$$\frac{\partial D_k}{\partial \sigma_{ij_k}^{(\ell)}} \approx \frac{\Delta D_k}{\Delta \sigma_{ij_k}^{(\ell)}} = \frac{D_k\left(\sigma_{ij_k}^{(\ell)} + \Delta\sigma_{ij_k}^{(\ell)}\right) - D_k\left(\sigma_{ij_k}^{(\ell)}\right)}{\Delta \sigma_{ij_k}^{(\ell)}}. \tag{20}$$

This scheme leads to sufficiently stable finite difference values as presented in Section 4.1. This approach is still numerically efficient since the finite difference evaluations are on material point level and the damage calculations at the material

points are uncoupled. Consequently, this leads to three additional fatigue damage evaluations for two-dimensional (2D) models due to σ_{11}, σ_{22}, and σ_{12} and six additional calls for three-dimensional (3D) structures due to σ_{11}, σ_{22}, σ_{33}, σ_{12}, σ_{23}, and σ_{13}. Fortunately, no additional structural solution of the residuum or adjoint equations are required for (20).

Hence, using the finite differences at the material points and exploiting that the partial damage derivatives w.r.t. $\boldsymbol{\phi}$ are zero, the sensitivities for fatigue damage at material point k are obtained using the following semi-analytical adjoint system

$$\frac{\mathrm{d}D_k}{\mathrm{d}\boldsymbol{\phi}} = \sum_{\ell=1}^{L}\left[\frac{\Delta D_k}{\Delta\sigma_{ij_k}^{(\ell)}}\frac{\partial\sigma_{ij_k}^{(\ell)}}{\partial\boldsymbol{\phi}} + \boldsymbol{\lambda}^{(\ell)\top}\frac{\mathrm{d}\boldsymbol{K}}{\mathrm{d}\boldsymbol{\phi}}\boldsymbol{u}^{(\ell)}\right]. \tag{21}$$

$$\boldsymbol{K}\boldsymbol{\lambda}^{(\ell)} = -\left(\frac{\Delta D_k}{\Delta\sigma_{ij_k}^{(\ell)}}\frac{\partial\sigma_{ij_k}^{(\ell)}}{\partial\boldsymbol{u}^{(\ell)}}\right)^{\top} \quad \text{where} \quad \ell = 1, 2, \dots, L. \tag{22}$$

We conclude that the derived semi-analytical fatigue sensitivities in Equations (19) and (21) are for fatigue calculations based on multiple load cases leading to multiple adjoint right hand sides for a single fatigue design response but uncommonly leads to the summation over the load cases for the single fatigue sensitivity. Secondly, the adjoint right-hand sides for Equation (22) is determined using a synthesis given by analytical derivatives of the stress tensor for the displacement fields and given by numerical derivatives of the fatigue damages for the stress tensors of the load cases.

3.4 | Aggregation function for approximating the maximum fatigue damage value

As previously stated fatigue damage D_k is evaluated at each material point $k \in \{1, 2, \dots, K\}$ where K is the total number of material points. Since we are interested in minimizing the maximum damage an aggregation function Ψ is applied to map the local damages D_k to a global maximum damage measure which is continuous and differentiable. Here we use the well known P-mean norm function for aggregation

$$\Psi_{\mathrm{PM}}(D_k) = c\left[\frac{1}{K}\sum_{k=1}^{K}(D_k)^p\right]^{\frac{1}{p}}, \tag{23}$$

where c is used for improving the approximation of the true maximum value.[10,11,37] However, the proposed method is not limited to a special aggregation function. Thus, the aggregation function is written as $\Psi(D_k)$. Thereby, the only change in sensitivity calculation is an additional term being the partial derivative of the aggregation function w.r.t. each aggregated damage value. The sensitivities applied for fatigue damage design optimization are then calculated as follows:

$$\frac{\mathrm{d}D}{\mathrm{d}\boldsymbol{\phi}} = \sum_{\ell=1}^{L}\left[\sum_{k=1}^{K}\left(\frac{\partial\Psi}{\partial D_k}\frac{\Delta D_k}{\Delta\sigma_{ij_k}^{(\ell)}}\frac{\partial\sigma_{ij_k}^{(\ell)}}{\partial\boldsymbol{\phi}}\right) + \boldsymbol{\lambda}^{(\ell)\top}\frac{\mathrm{d}\boldsymbol{K}}{\mathrm{d}\boldsymbol{\phi}}\boldsymbol{u}^{(\ell)}\right]. \tag{24}$$

$$\boldsymbol{K}\boldsymbol{\lambda}^{(\ell)} = -\left(\sum_{k=1}^{K}\frac{\partial\Psi}{\partial D_k}\frac{\Delta D_k}{\Delta\sigma_{ij_k}^{(\ell)}}\frac{\partial\sigma_{ij_k}^{(\ell)}}{\partial\boldsymbol{u}^{(\ell)}}\right)^{\top} \quad \text{where} \quad \ell = 1, 2, \dots, L. \tag{25}$$

4 | NUMERICAL IMPLEMENTATION

As previously described the optimization is performed using mathematical programming being an iterative design optimization approach. The implemented optimization workflow is shown in Figure 5. The optimization framework and mathematical programming is implemented using *Tosca Structure*.[38] The damage values for the sensitivities are evaluated at the element integration points.

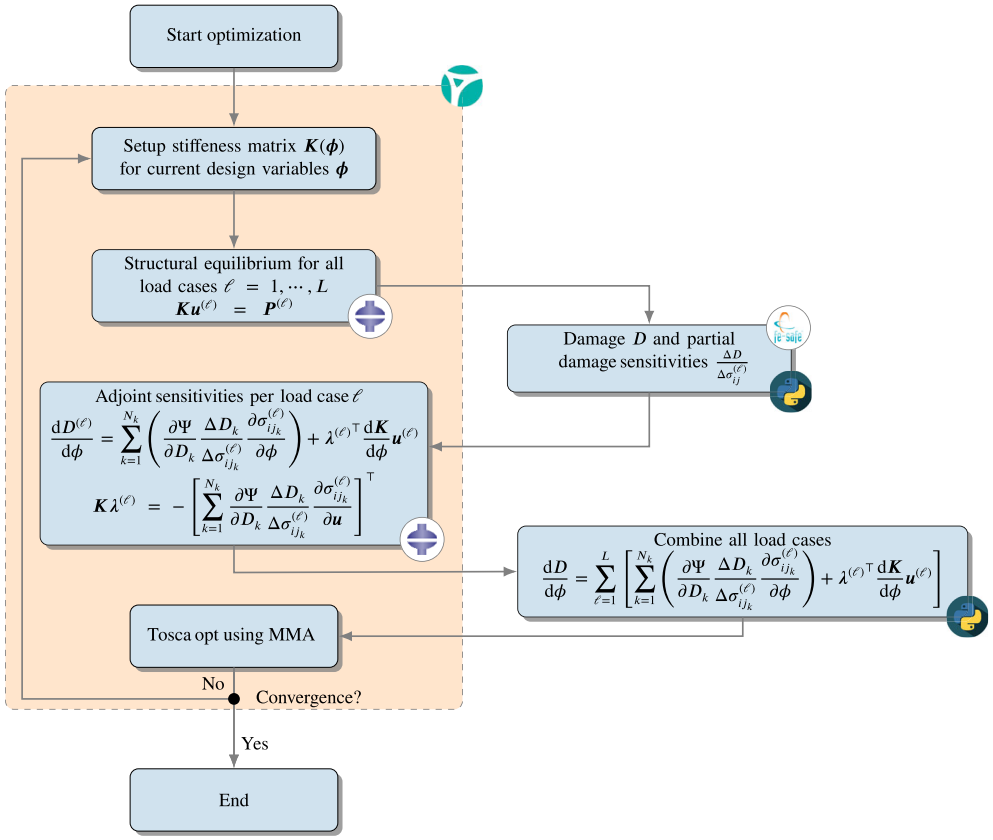

FIGURE 5 Flowchart of the design optimization workflow using numerical partial damage sensitivities for the adjoint sensitivity calculation

The FEA is solved with *Abaqus/Standard*.[39] The calculated stresses are then used in the fatigue analysis software *fe-safe*[19] to perform fatigue damage calculation. For partial finite difference sensitivities, the stress tensors are perturbed in each tensor direction and evaluated again with *fe-safe*. In an additional *Abaqus* FE-calculation, the adjoint sensitivities are calculated for each load case. Finally, these values are summed up to obtain the sensitivities used for the sensitivity based design update. The optimization procedure is repeated until the convergence criteria are fulfilled.

Typically, the *Abaqus* FE-solver is only applied once to calculate both the structural design response and the adjoint sensitivities for one optimization iteration cycle. In contrast, the present implementation requires the stresses for calculating the partial fatigue damage sensitivities, and, hence, requires a second *Abaqus* FE-evaluation to calculate the adjoint sensitivities. The present implementation requires a modification of the pseudo load vector with the partial fatigue damage sensitivities. Hence, Abaqus is called a second time to calculate the adjoint solution.

We use the Method of Moving Asymptotes[40] to update the design variables. Once the design variables are updated, the algorithm loops back to the evaluation of the objective and constraint functions if the stopping criteria are not fulfilled.

Two criteria are tested to check convergence: the relative change of the objective function must be below 0.1% and the relative change of the design variables must be below 0.5%.

4.1 | Validation of the finite difference step size for fatigue damage

This work relies on the finite difference approximation of the fatigue damage sensitivities for the damage parameters including critical plane search and rainflow counting. Therefore, we have to validate that the finite difference approximations $\frac{\Delta D}{\Delta \sigma_{ij}}$ for the partial derivatives $\frac{\partial D}{\partial \sigma_{ij}}$ is sufficiently accurate. For this purpose two load histories are considered, as shown in Figure 6. The material data is given in Table 1 and the Brown–Miller damage parameter is applied including the critical plane analysis.

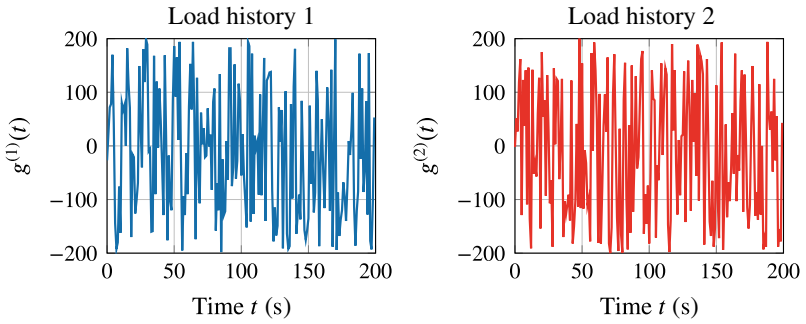

FIGURE 6 Load histories for time history calculation according to Equation (5)

TABLE 1 Material data applied for fatigue damage calculation

E	ν	σ'_f	b	ε'_f	c
203,000 MPa	0.33	930 MPa	−0.095	0.26	−0.47

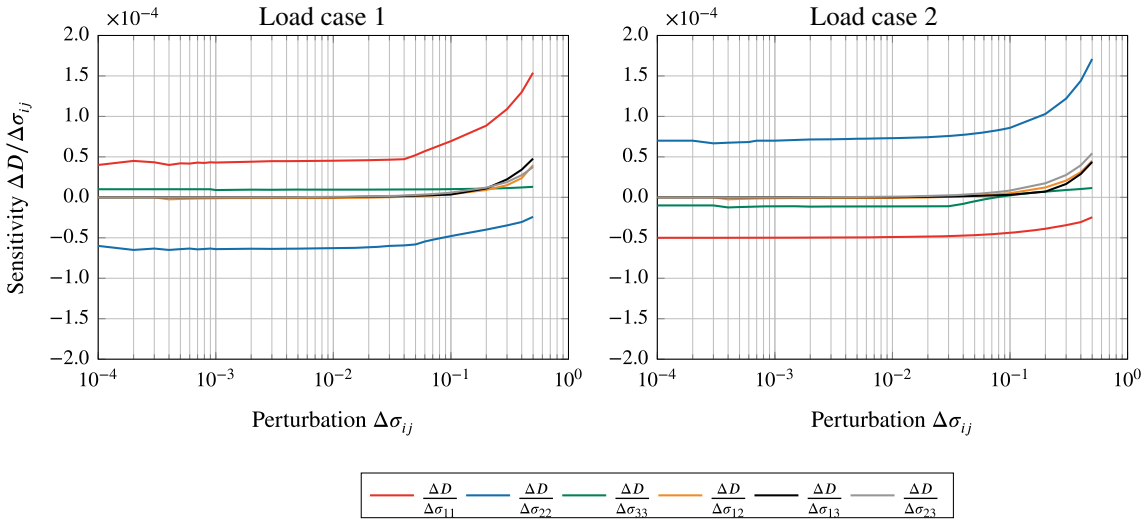

FIGURE 7 Finite difference derivatives for different perturbation sizes $\Delta\sigma_{ij}$ based on the *Brown–Miller* damage parameter. (A) Load case one $\boldsymbol{\sigma}^{(1)} = \begin{bmatrix}1 & 0 & 0 & 0 & 0 & 0\end{bmatrix}^\top$ and (B) load case two $\boldsymbol{\sigma}^{(2)} = \begin{bmatrix}0 & 1 & 0 & 0 & 0 & 0\end{bmatrix}^\top$ having the load histories shown in Figure 6.

In Figures 7 and 8 show the validation results for both uniaxial and multiaxial stress states are shown. The finite difference values converge to a stable value in the mid range but are numerically unstable for too small small stress variations $\Delta\sigma_{ij}$. Note, that this was also tested for other damage parameters and other stress states showing similar behavior. Therefore, we conclude that the numerical differentiation approximating the partial fatigue damage derivatives w.r.t. to the stress tensor is practically applicable for engineering applications.

Perturbations of $\Delta\sigma_{ij} = 0.01 \cdots 0.001\sigma_{\max}$ lead to sufficiently accurate results, where $\sigma_{\max}$ is the absolute maximum entry of the stress tensor. Consequently, a perturbation size of $\Delta\sigma_{ij} = 0.001\sigma_{\max}$ is chosen for the present work.

4.2 | Global finite difference validation

After validating the partial fatigue damage sensitivities the next step is to validate the semi-analytical adjoint sensitivities and, hence, corresponding the overall workflow shown in Figure 5. This is achieved by comparing the adjoint sensitivity

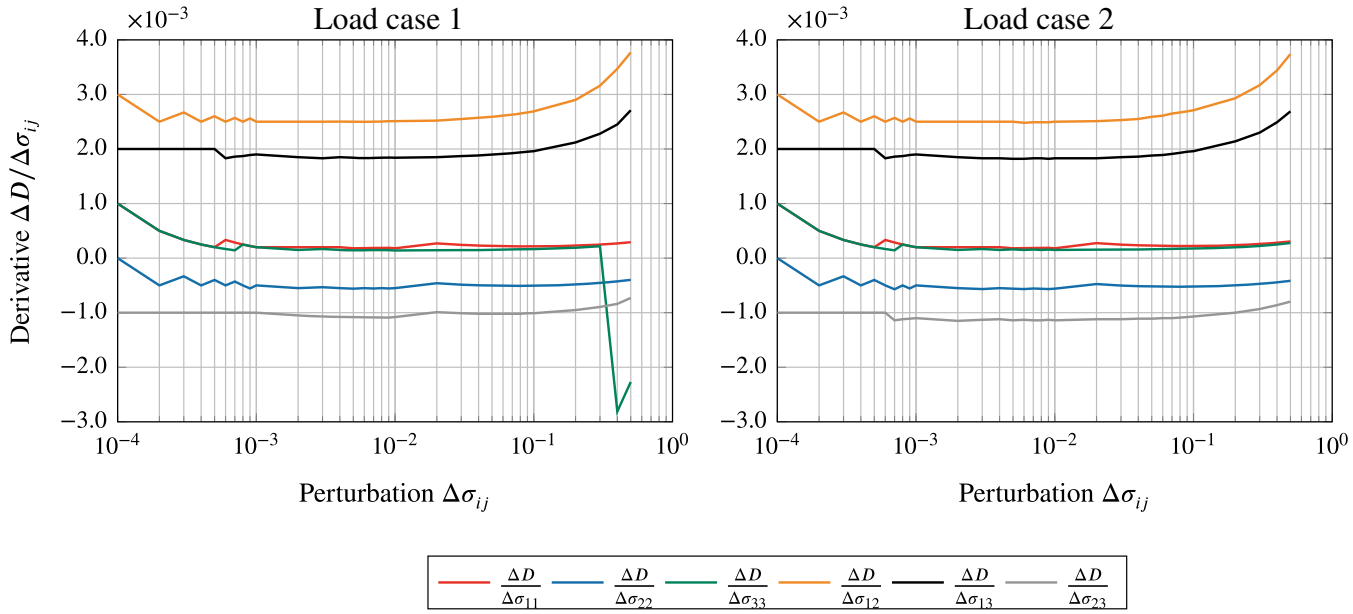

FIGURE 8 Finite difference derivatives for different perturbation sizes $\Delta\sigma_{ij}$ based on the *Brown–Miller* damage parameter . (A) Load case one $\boldsymbol{\sigma}^{(1)} = \begin{bmatrix}0.58 & -0.35 & 0.95 & 0.88 & 0.09 & 0.67\end{bmatrix}^\top$ and (B) load case two $\boldsymbol{\sigma}^{(2)} = \begin{bmatrix}0.15 & 0.17 & -0.23 & 0.71 & -0.84 & 0.45\end{bmatrix}^\top$ having the load histories shown in Figure 6.

w.r.t. one design variable $\phi \in \boldsymbol{\phi}$ to the finite difference approximation for $\frac{\Delta D}{\Delta \phi}$. The finite difference approximation is calculated using the central finite difference method

$$\frac{\Delta D}{\Delta \phi} = \frac{D(\phi + \Delta\phi) - D(\phi - \Delta\phi)}{2\Delta\phi}. \tag{26}$$

The model used for validation is shown in Figure 9. It consists of four-node shell elements (S4) having four integration points in plane and five section points in the thickness direction, that is, 20 integration points in total. However, for fatigue damage evaluation only integration points at the top and bottom surface are considered, that is, eight integration points in total. The structure is clamped at two corner nodes and two load cases are applied at a third corner node. The highlighted element is used for the damage evaluation. The thickness t of the same element is considered as design variable to validate sizing optimization. The highlighted node is used for validating the nodal positions x, y and z as design variable. The damage value is the average over all integration points.

To perform validation for realistic data set the load histories (shown in Figure 9) are based on measurements from real world applications. The material data that is used for this model is provided in Table 1. The ratio R defines the accuracy between the semi-analytical adjoint sensitivities and the finite difference approximation

$$R = \frac{\mathrm{d}D}{\mathrm{d}\phi} \Big/ \frac{\Delta D}{\Delta \phi}. \tag{27}$$

The adjoint sensitivities are valid if R is close to one.

The validation results are summarized in Table 2. As the ration R is close to one, the approach for approximating the adjoint sensitivities and, hence, the total optimization workflow is validated. Therefore, we conclude that the proposed method has sufficient accuracy for calculating sensitivities in realistic engineering scenarios.

We observe that the rainflow counting rarely changes in the finite difference step. Several other numerical experiments for different stress states were conducted showing the same observations. This is also in agreement with the common assumption in the literature stating that the rainflow counting is constant when deriving adjoint sensitivities.[7,11,14] However, the approach presented in this paper allows us for the first time to numerically prove this assumption for various damage parameters.

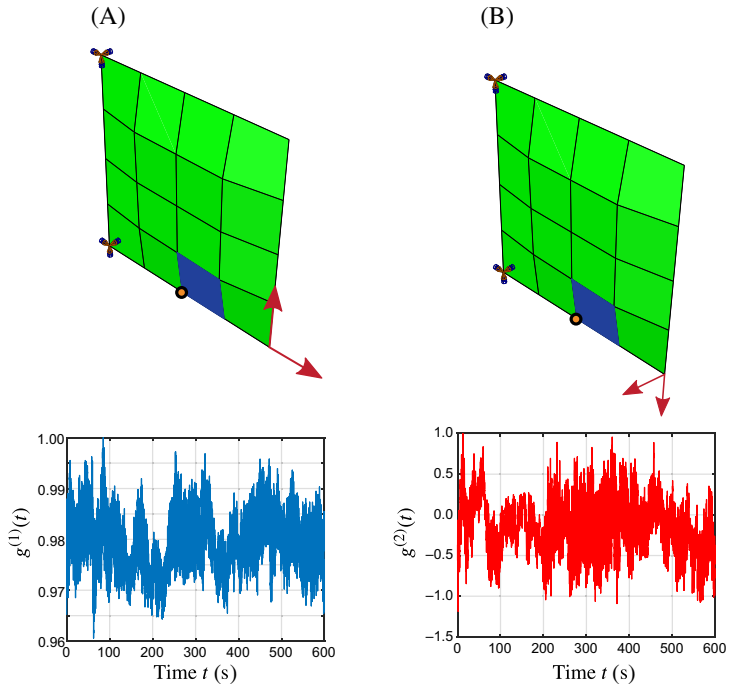

FIGURE 9 Shell model considered for the finite difference validation of semi-analytical adjoint sensitivities. Two load cases with different load histories are applied. (A) Load case 1 is in-plane loading. (B) Load case 2 is out of plane loading. The force is applied as point load at the lower right corner node. The highlighted element is used for fatigue damage evaluation and sizing design variable sensitivity validation. The highlighted node is chosen for nodal position sensitivity validation.

TABLE 2 Finite difference validation of adjoint sensitivities for different design variable types

Design variable ϕ	Adj. Sens	$D(\phi + \Delta\phi)$	$D(\phi - \Delta\phi)$	Fin. diff.	Accuracy R
x	2.23E-03	1.05E-03	1.05E-03	2.25E-03	**0.99**
y	1.06E-02	1.05E-03	1.05E-03	1.06E-02	**1.00**
z	7.70E-03	1.05E-03	1.05E-03	7.75E-03	**0.99**
t	-3.91E-02	1.04E-03	1.05E-03	-3.89E-02	**1.01**

Notes: In all cases the Brown–Miller damage parameter is applied, thus, critical plane search is included. Each design variable is perturbed by $\Delta\phi = 0.001$.

5 | NUMERICAL EXAMPLES

The numerical examples presented in this paper show the applicability of the proposed method for different optimization setups and applications ranging from small academic examples to large scale examples. Three aspects are investigated in the examples:

1. **Different damage parameters:** Applying different damage parameters for design optimization to compare their impact on the design as well as for comparison with designs from static stress-based optimization.
2. **Different design variables:** Optimization using shape, sizing, and bead design variables, as shown in Table 4.
3. **Different optimization formulations:** Optimization setups with and without volume constraint, application of fatigue damage either as objective or as constraint.

5.1 | L-bracket shape optimization example—different damage parameters

The L-bracket example is identical to the one discussed in the introduction (Figure 1). The structure is discretized using two different finite element types: six-node wedge elements with two integration points (C3D6) and eight-node hexahedral elements with eight integration points (C3D8). In total the structure consists of 2144 elements. Fatigue

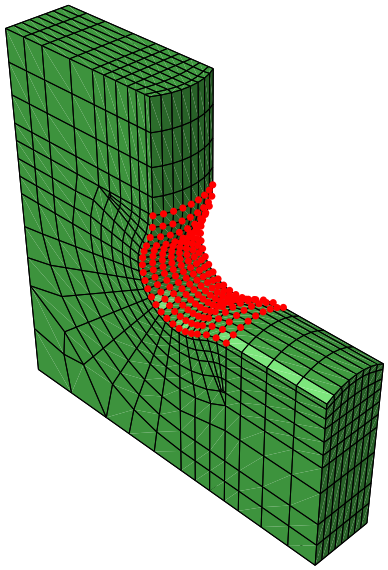

FIGURE 10 Design nodes for the shape optimization of the L-bracket

damage is evaluated at the integration points of 956 elements at the outer surface of the bracket. The design nodes consist of 198 surface nodes in the corner area as shown in Figure 10. According to Figure 4B the nodal position is chosen as design variable. Additionally, a mesh smoothing algorithm is applied to avoid sharp transitions at the design domain boundary. A regularization filter as described in Equations (11) and (12) with a filter size of one average element edge length is chosen.

Two load cases are applied: one with high stresses but a low frequency in the time history and a second load case having lower stresses at a high frequency in the time history. The material properties for this example are the same as for the validation model given in Table 1. The optimization task is defined by minimizing the maximum damage D, that is, $g_0 = D$. Four different damage parameters are considered: Brown–Miller, Normal Strain, Normal Stress including Morrow[41] MSC and von Mises Stress including Goodman[42] MSC. Moreover, for comparison the static stress-based optimization of minimizing the maximum von Mises stress of all load cases $\sigma^{(\ell)}_{\text{Mises}}$ written as

$$g_0 = \max\left(\sigma^{(\ell)}_{\text{Mises}}\right) \quad \text{where} \quad \ell = 1, 2. \tag{28}$$

The MIN-MAX formulation over the load cases applied to Equation (28) for maximum stress- or compliance-based objective functions Equation (7) is solved as a standard optimization problem in which the objective function is remodelled into a set of constraints using the bound formulation.[43,44] The same method is applied to all MIN-MAX formulations in the present work. The MIN-MAX formulation over the load cases is not required for the fatigue damage optimization as the stresses of the multiple load cases are superposed using the load histories as defined in Equation (5).

The optimization results are summarized in Table 3. The first column shows the fatigue damage distribution of the initial design. As expected the fatigue damage hotspot is different from the location of maximum static stress. In each subsequent column the optimized design for the different damage parameter types are evaluated applying the different damage parameter types. Thus, ideally the highlighted cell should have the lowest fatigue damage value for a given damage parameter in each row. This holds true for all but the von Mises damage parameter. In this case the normal stress optimized design shows a slightly lower maximum fatigue damage value. Conceivably this is caused by the optimization iteration histoy of the normal stress designing that requires twice the amount of optimization iterations for the present application before the stop criteria for the relative change of the design variables are fulfilled.

The percentage values in parenthesis in the diagonal boxes shows the maximum fatigue damage value of the optimized design in relation to the initial damage value, that is, the ratio $\frac{D^{\text{opt}}}{D^{\text{initial}}}$. For all damage parameters the maximum fatigue damage values are significantly reduced. This example highlights that the optimization approach is generally capable of handling different damage parameter types.

TABLE 3 Shape of optimized designs for different damage parameter types as well as for static stress optimization

Evaluation Damage Parameter	Initial Damage	Optimization Damage Parameter: Brown-Miller	Normal Strain	Normal Stress	Von Mises Stress	$\min\max(\sigma^{(\ell)}_{\text{Mises}})$	Legend
Iter.	0	23	30	40	26	13	
Brown-Miller	Max=17.55 × 10^{-3}	**Max=**2.05 × 10^{-3} **(12%)**	Max=2.20 × 10^{-3}	Max=2.27 × 10^{-3}	Max=2.32 × 10^{-3}	Max=12.60 × 10^{-3}	Damage 0.0027 0.0025 0.0023 0.0020 0.0018 0.0016 0.0014 0.0011 0.0009 0.0007 0.0005 0.0002 0.0000 -0.0002
Normal Strain	Max=11.07 × 10^{-3}	Max=1.48 × 10^{-3}	**Max=**1.19 × 10^{-3} **(11%)**	Max=1.29 × 10^{-3}	Max=1.32 × 10^{-3}	Max=8.10 × 10^{-3}	Damage 0.0015 0.0014 0.0013 0.0011 0.0010 0.0009 0.0008 0.0006 0.0005 0.0004 0.0003 0.0001 0.0000 -0.0001
Normal Stress	Max=25.08 × 10^{-3}	Max=3.24 × 10^{-3}	Max=2.47 × 10^{-3}	**Max=**2.08 × 10^{-3} **(8%)**	Max=2.46 × 10^{-3}	Max=17.95 × 10^{-3}	Damage 0.0091 0.0083 0.0076 0.0068 0.0061 0.0053 0.0046 0.0038 0.0030 0.0023 0.0015 0.0008 0.0000 -0.0012
Von Mises Stress	Max=13.06 × 10^{-3}	Max=1.87 × 10^{-3}	Max=1.81 × 10^{-3}	Max=1.52 × 10^{-3}	**Max=**1.53 × 10^{-3} **(12%)**	Max=10.00 × 10^{-3}	Damage 0.0063 0.0058 0.0053 0.0047 0.0042 0.0037 0.0032 0.0026 0.0021 0.0016 0.0011 0.0005 0.0000 -0.0012

Notes: The table includes a crossover check for the optimized shapes. Each column refers to an optimized design obtained from an optimization based on the given damage parameter. Each row corresponds to the damage parameter used for evaluation.

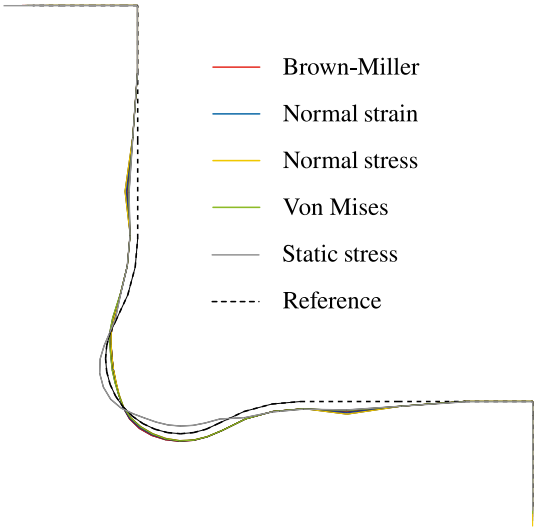

FIGURE 11 Mid-surface of the optimized shapes for different damage parameters

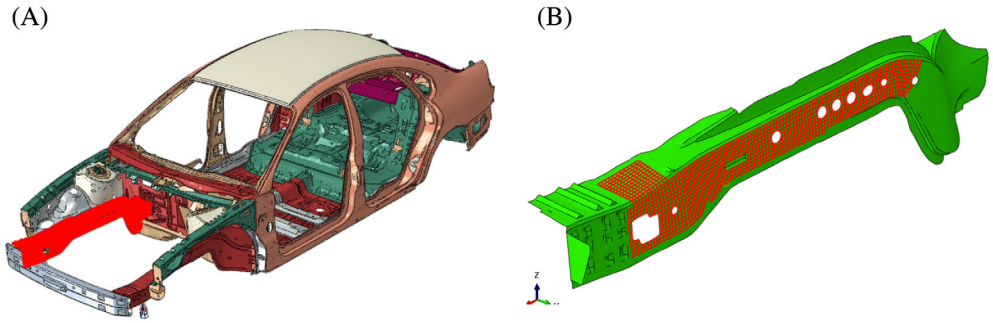

FIGURE 12 (A) Full body in white model used for the finite element-simulation of each optimization iteration. (B) Design space considered for the design optimization and for the fatigue damage evaluation.

The mid-surfaces for the optimized shapes are shown in Figure 11 indicating that there are only minor differences. However, since fatigue damage is a highly local quantity depending on local differences in the design the calculated fatigue damage is different for all designs. This shows that fatigue damage is highly dependent on small variations of the design.

For comparison, the last column of Table 3 shows results from the static stress-based optimization. Again, the optimized design leads to a reduction in fatigue damage, but the change is less significant. When compared with the approach for fatigue damage optimization proposed in this paper, the increase in lifetime is less by a factor of about 10.

5.2 | Body in white—different design variables and optimization setups

In this example we examine two different design variable types: sizing thickness design variables (see Figure 4A) nodal bead design variables (see Figure 4C).

The finite element model is shown in Figure 12A. It consists of 354,182 elements and about 2.2×10^6 degrees of freedom. The full FE-model is evaluated in each optimization iteration in order to capture the correct interface forces between all components. However, only the highlighted subsection of the front side member consisting of 1103 elements (1273 nodes) is considered (see Figure 12B). Nodal positions and element thicknesses are chosen as design variables for bead and sizing optimization, respectively. The front side member is discretized using fully integrated shell elements (S4) with four integration points in the plane and five section points in thickness direction as well as triangular shell elements with reduced integration order (S3R) having one integration point in the plane and five section points in the thickness. Fatigue damage is evaluated on the top and bottom section points, that is, eight (S4) and two (S3R) material points are considered for fatigue damage calculations, respectively.

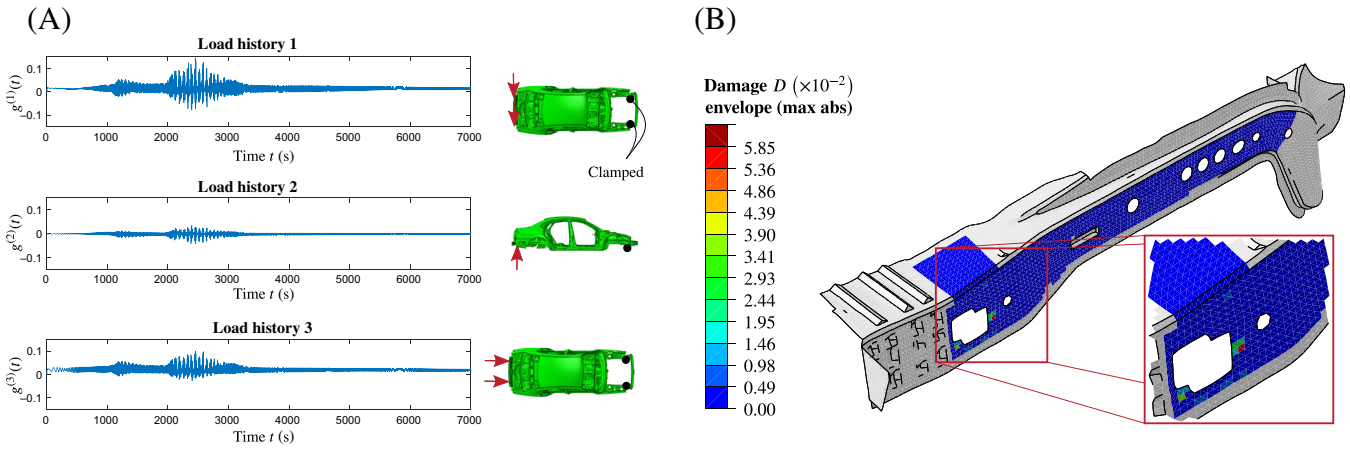

FIGURE 13 (A) Applied load histories and load conditions for the body in white model. (B) Damage contour plot of the initial design

For bead optimization, the design variables are constrained by a lower bound $\Delta\boldsymbol{\varphi}^{\mathrm{L}} = -0.5\,\mathrm{mm}$ in the negative normal direction and an upper bound $\Delta\boldsymbol{\varphi}^{\mathrm{U}} = 5\,\mathrm{mm}$ in the positive normal direction. The regularization filter is applied with a filter size of two average element edge lengths. Similarly, the sizing thicknesses are restricted to a lower bound of $\boldsymbol{\varphi}^{\mathrm{L}} = 0.2\boldsymbol{\varphi}_0$ and an upper bound $\boldsymbol{\varphi}^{\mathrm{U}} = 2\boldsymbol{\varphi}_0$ in relation to the initial thickness distribution $\boldsymbol{\varphi}_0$. The sizing optimization uses a regularization with a filter radius of 30 mm. Sizing optimization is performed with and without a volume constraint.

The load histories applied for the fatigue damage calculations and the corresponding load conditions are shown in Figure 13A. The car is clamped at the front end and the load is applied at two nodes at the rear end. Note again, that the structural response is computed for the full model in each optimization iteration.

For the fatigue damage calculations the Brown–Miller damage parameter is applied including critical plane analysis and Morrow MSC. In Figure 13B the fatigue damage distribution of the initial design is shown. High damage values occur only at a few elements while significant portions of the design space have low damage values.

5.2.1 | Fatigue damage as objective

In this section the objective function for Equation (7) is defined by the accumulated fatigue damage

$$g_{0,D} = D. \tag{29}$$

A volume constraint $g_1 = \frac{V}{V_0} \leq 1$ ensures that the initial mass of the structure is not exceeded. For comparison two stress based optimizations are performed in addition to the fatigue based optimization, by minimizing the maximum von Mises stress and the first principal stress of all load cases:

$$g_{0,\mathrm{Mises}} = \max\left(\sigma^{(\ell)}_{\mathrm{Mises}}\right), \text{ where } \ell = 1,2,3, \tag{30}$$

$$g_{0,\sigma_1} = \max\left(\sigma^{(\ell)}_{1}\right), \text{ where } \ell = 1,2,3. \tag{31}$$

Table 4 shows the optimized designs for the different optimization formulations. Even though the unconstrained sizing optimization leads to an increase in mass of 8% the maximum fatigue damage value observed in this design is higher than in the optimized design from a sizing optimization with volume constraint. This indicates that the unconstrained optimization converges to a local optimum. Nevertheless, this example shows that the proposed fatigue damage optimization works properly in combination with an additional volume constraint.

The optimization history plots in Table 4 show that the maximum fatigue damage is consistently decreasing over the optimization iterations. Therefore, we conclude that the adjoint sensitivities for fatigue damage with respect to various design variable types (bead and sizing thickness design variables) are numerically reliable and applicable to typical engineering problems.

Table 5 summarizes the results from the static stress based optimizations subject to a mass volume constraint and compares them to the design optimized for fatigue. Both the stress-based and the fatigue damage optimizations show a stable

TABLE 4 Optimized designs of the body in white front side member and corresponding optimization convergence plots

Optimization	Bead	Sizing	Sizing s.t. volume constraint
D	1.48×10^{-2}	5.41×10^{-3}	1.84×10^{-3}
Iter	63	41	69
Design changes $\Delta\boldsymbol{\phi}$	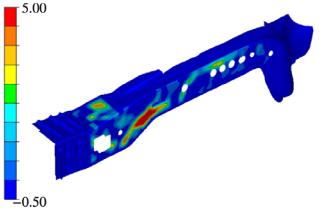	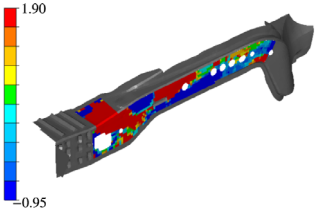	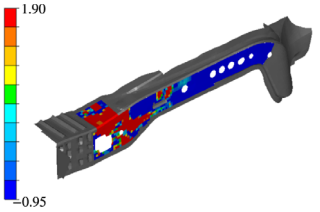
Damage	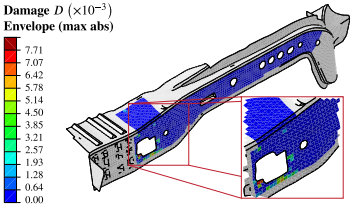	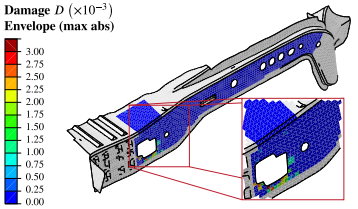	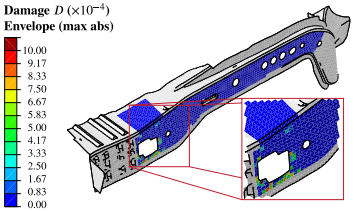
Optimization convergence plot	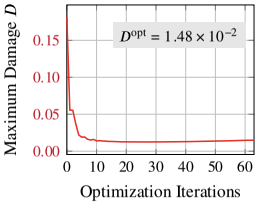	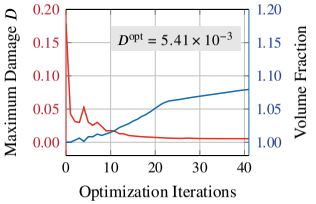	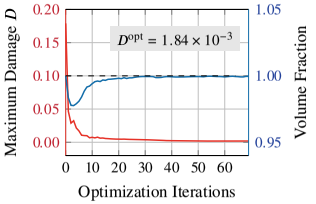

TABLE 5 Comparison of stress- and fatigue-based sizing optimizations subject to a volume constraint

Optimization	Fatigue damage	Static Von Mises stress	Static first principal stress
D	$\underline{1.84 \times 10^{-3}}$	15.43×10^{-3}(~ ×8.4)	17.19×10^{-3}(~ ×9.3)
σ_{Mises}	5602 (~ ×0.98) MPa	$\underline{5700\ \text{MPa}}$	6783 MPa (~ ×1.19)
σ_1	6047 MPa (~ ×1.11)	6286 MPa (~ ×1.03)	$\underline{6098\ \text{MPa}}$
Iter.	69	20	32
	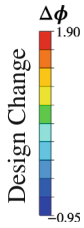	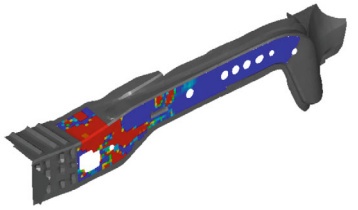		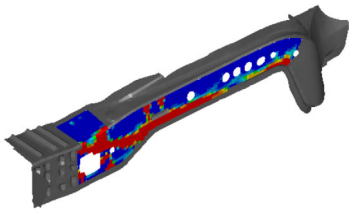
	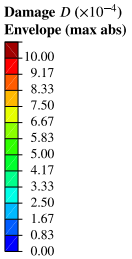	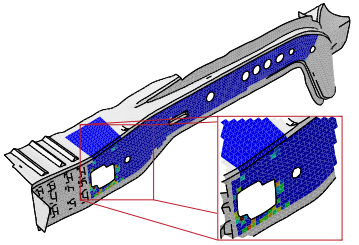	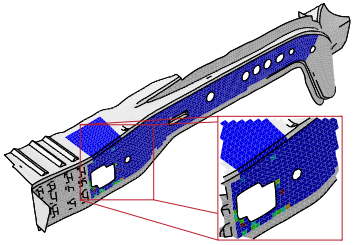	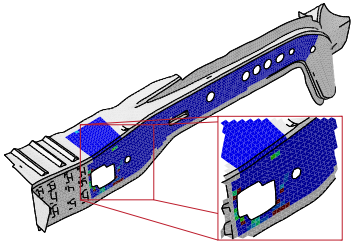
Optimization convergence plot	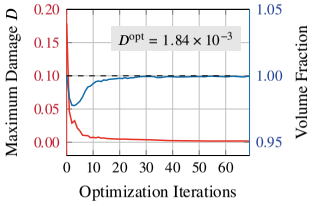	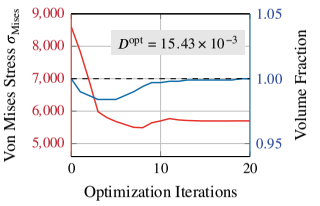	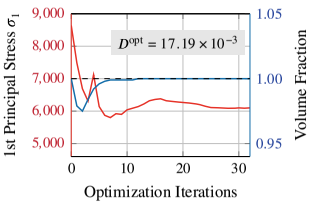

TABLE 6 Optimized designs for minimized mass subject to fatigue damage constraint

D_{max}	5×10^{-3}	2×10^{-3}
V/V_0	54%	74%
D	4.77×10^{-3}	2.01×10^{-3}
Iter.	50	83
Design Change		
Damage	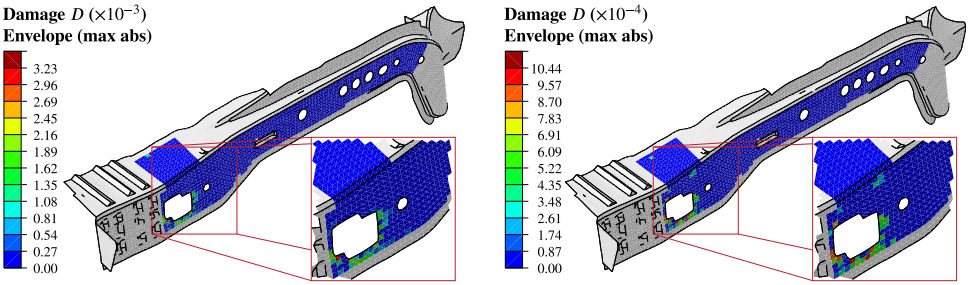	
Optimization convergence plot	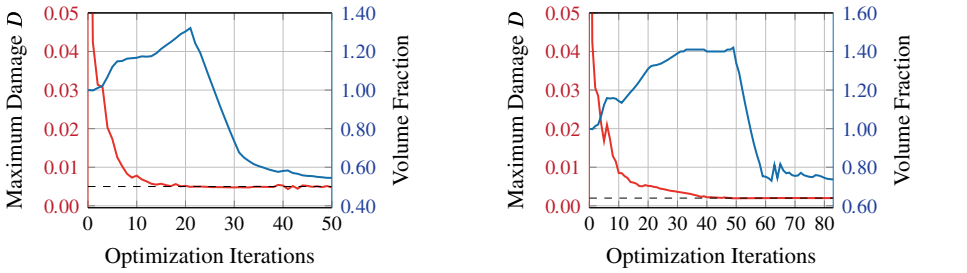	

optimization convergence. In the iterature proportional fatigue damage optimization problems are often converted into a stress-based optimization problem using 1st principal stresses or von Mises stresses.[7] However, the crossover check in Table 5 shows that this is not a valid optimization approach for non-proportional fatigue damage as the maximum fatigue damage for the design optimized based on the first principal stresses is 9.3 times higher than the design directly optimized for non-proportional fatigue damage. Similarly, the design optimized based on von Mises stresses has a maximum fatigue damage value being 8.4 times higher than the design directly optimized for nonproportional fatigue damage.

5.2.2 | Fatigue damage as constraint

So far the numerical examples had the fatigue damage as objective function. In the following optimization we define the fatigue damage as a constraint for sizing optimization where the objective is to minimize the mass or volume, respectively, that is, $g_0 = V$ and having the damage as constraint $g_1 = D \leq D_{max}$. The material properties and the model are the same as in the previous optimization.

The sizing optimized designs are shown in Table 6. Many thickness design variables have the lower bound thickness in the final optimized design to reduce the mass. The convergence plots show that the optimization successfully reduces the initial mass of the part while fulfilling the fatigue damage constraint.

Based upon the present optimization results, then we conclude that the proposed semi-analytical adjoint sensitivities work practically also when the fatigue damage is considered as constraint and not only as objective.

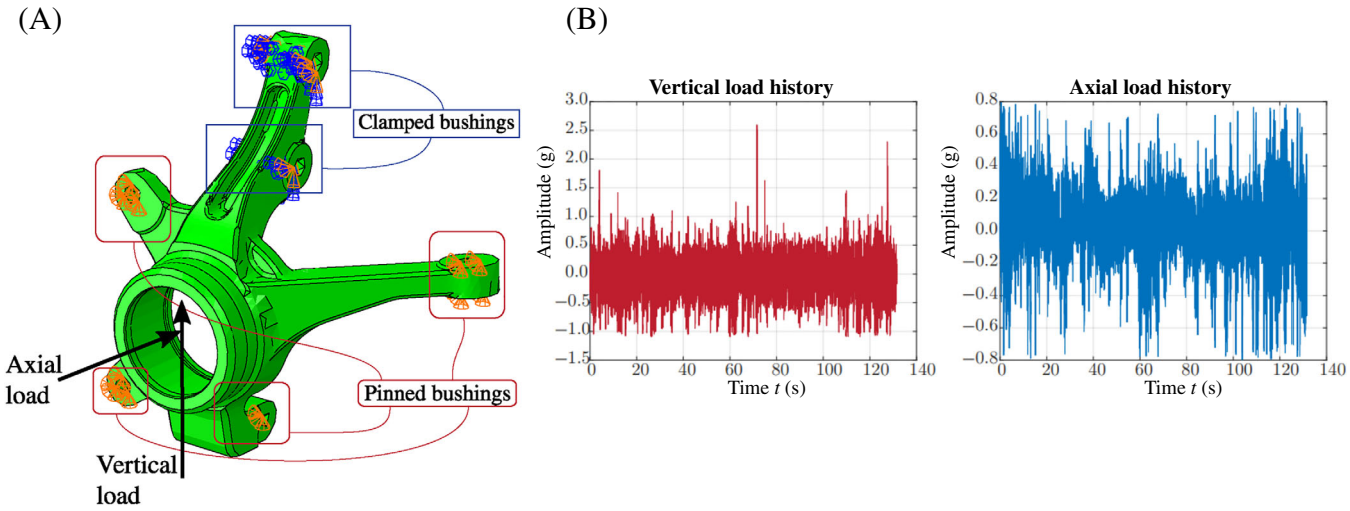

FIGURE 14 (A) Boundary and load conditions for the steering knuckle. (B) Load histories for the fatigue calculation

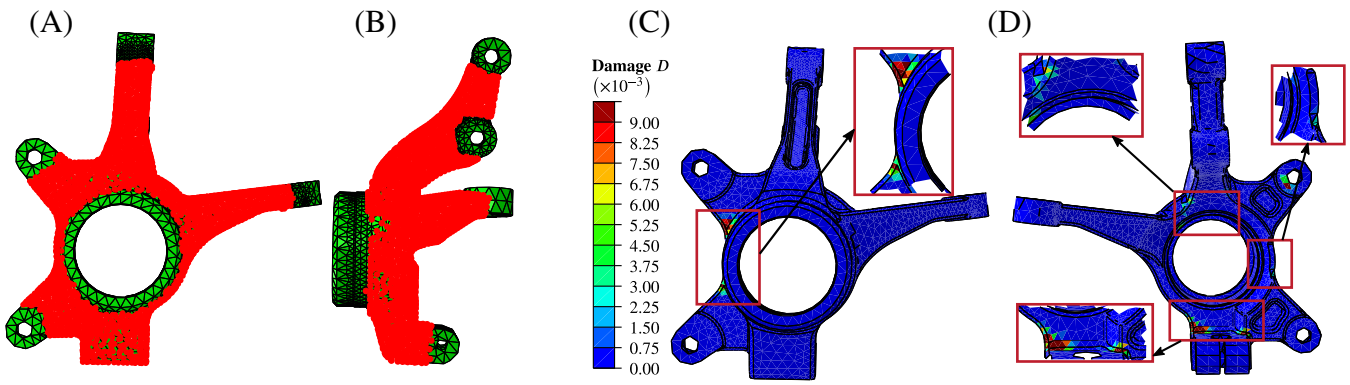

FIGURE 15 (A,B) Design nodes for the non-parametric shape optimization of the steering knuckle. (C,D) Damage contour of the initial design. The legend is the same as in Table 8.

TABLE 7 Material data for fatigue damage calculation

E	ν	σ'_f	b	ε'_f	c
70,000 MPa	0.33	594 MPa	−0.124	0.027	−0.53

5.3 | Steering knuckle shape optimization—different optimization formulation

Finally, a shape optimization is performed for a steering knuckle as shown in Figure 14A. The structure is discretized using 44,347 elements being four-node tetrahedral continuum elements (C3D4) having one integration point. Figure 15A,B shows the 4419 nodes at the surface that are chosen as design variables for the shape optimization (compare Figure 4B). The material properties are listed in Table 7. In contrast to the previous example the Normal Strain damage parameter with Morrow MSC including critical plane analysis is applied to test another damage parameter that is, for example, used for cast metals. Again, mesh smoothing is applied to avoid sharp transitions between the design nodes of the design space and the non-design space. A regularization filter is chosen having a radius of two average element edge lengths. The holes are excluded from the mesh smoothing since they should remain unchanged ensuring that the connectivity remains to other structural parts for the final optimized assembly. The boundary conditions and the load cases are shown in Figure 14A. One load case represents an axial loading and another load case a vertical loading having the corresponding load histories as shown in Figure 14B. The loads are distributed over the entire surface of the center hole.

TABLE 8 Shape optimization results for the steering knuckle

	Fatigue Damage Optimization	Von Mises Stress Optimization	Compliance Optimization
Iter.	41	15	16
D	8.84×10^{-3}	25.06×10^{-3} ($\sim \times 2.8$)	174.80×10^{-3} ($\sim \times 20$)
σ_{Mises}	181MPa ($\sim \times 1.0$)	181 MPa	216MPa ($\sim \times 1.2$)
c	4041 ($\sim \times 1.1$)	4083($\sim \times 1.1$)	3740
Nodal Design Change	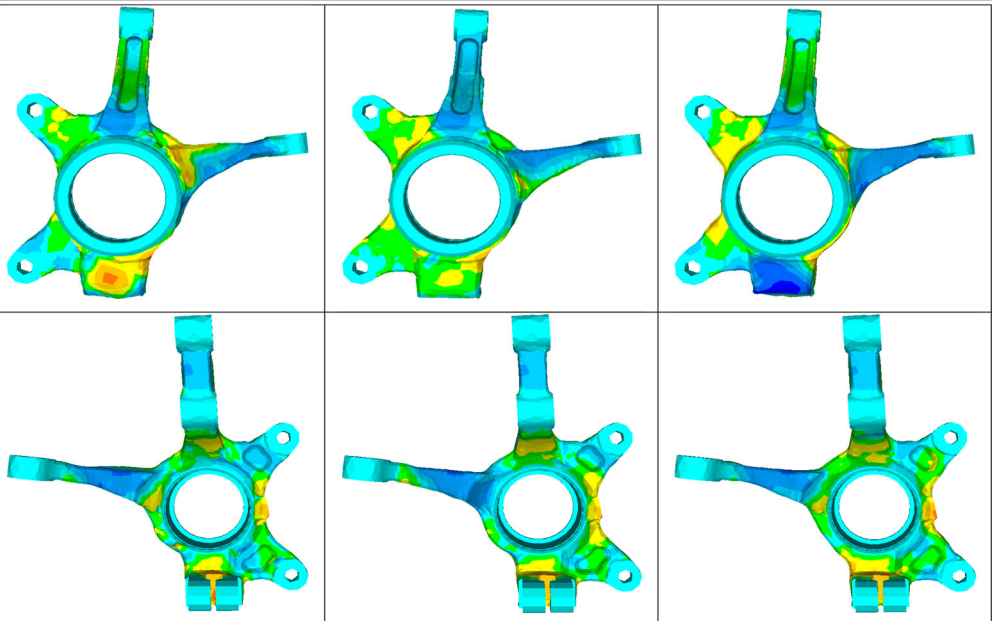		
Damage Contour	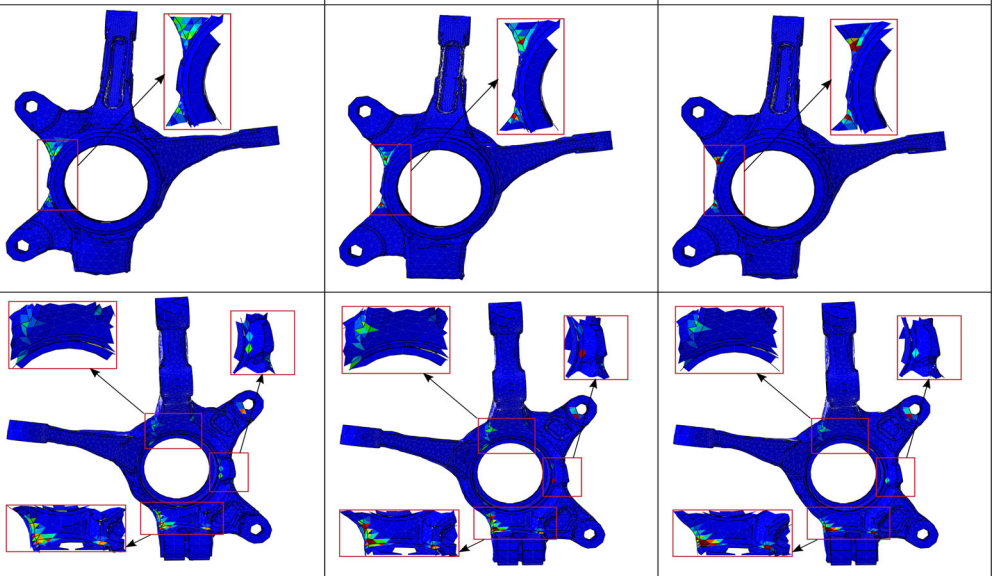		
Convergence history	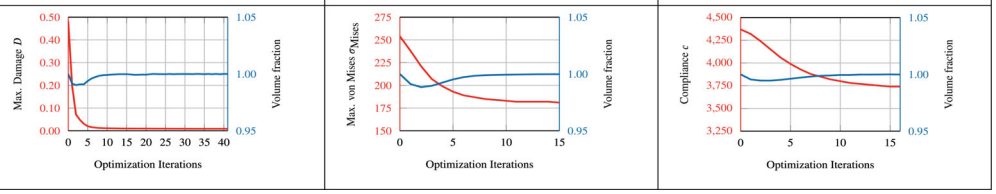		

Note: The values in the brackets show the relative comparisons to the specific optimized values.

Three different objective functions are considered for the present optimization to compare the fatigue optimized design with static stress design and stiffness optimized design. The applied objective functions are defined as the following:

$$g_{0,D} = D. \tag{32}$$

$$g_{0,\sigma} = \max\left(\sigma^{(1)}_{\text{Mises}}, \sigma^{(2)}_{\text{Mises}}\right). \tag{33}$$

$$g_{0,c} = \max\left(\boldsymbol{u}^{(1)\top}\boldsymbol{P}^{(1)}, \boldsymbol{u}^{(2)\top}\boldsymbol{P}^{(2)}\right). \tag{34}$$

The first objective $g_{0,D}$ is chosen to minimize the damage. The second objective $g_{0,\sigma}$ minimizes the maximum von Mises stress of the two load cases and the third objective $g_{0,c}$ minimizes the maximum compliance of the two load cases. All optimizations are subjected to a volume constraint, that is, $g_1 = \frac{V}{V_0} \leq 1$ conserving the mass of the initial design.

The optimized designs are shown in Table 8. The optimized shapes are clearly different. Both, the fatigue damage and the static von Mises stress optimized designs have a significant reduced maximum fatigue damage value. Interestingly, the fatigue damage optimized design has similar von Mises stresses compared to the static von Mises stress optimized result. However, the static stress optimized design has a maximum fatigue damage value being three times higher. Similarly, the worst fatigue damage obtained by stiffness optimization is 20 times higher then the fatigue damage of the fatigue damage optimized design. Again, we can numerically conclude that neither the stress optimized design nor the stiffness optimized design provide suitable damage values and for non-proportional fatigue damage the fatigue damage has to be directly included in the optimization formulation.

6 | CONCLUSION

Counterintuitive, we have derived and implemented a new approach for non-parametric optimization using semi-analytical adjoint sensitivities where all essential characteristics for representative fatigue damage calculations are included. This includes the two most important supported characteristics critical plane analysis and the rainflow-counting. Those are applied for nonproportional loading and cannot be differentiated using an analytical closed-form approach. The combination of these two important characteristics for fatigue damage calculations regarding optimization is neglected in previous works.

Mathematically, a fatigue damage calculated is not strictly differentiable. However, our numerical findings and experiments show that the partial derivatives of the fatigue damage with respect to the stress tensor is practically and realistically approximated for engineering applications. Thereby, the adjoint sensitivities for the fatigue damage with respect to the various types of design variables are calculated using the semi-analytical adjoint sensitivity approach.

The approximated partial derivatives of the fatigue damage with respect to the stress tensor for the semi-analytical adjoint sensitivities is calculated using finite difference of the stresses per load case for each material point. The numerical verification using the forward finite difference shows valid and consistent sensitivities for a 0.1% to a 1% stress variation. The approximated partial derivatives are calculated per material point being equal to the elemental integration points of the finite element model. Therefore, three and six stress forward finite differences for 2D and 3D are applied on material point level. Thus, the computational performance for the runtime of the forward finite differences is efficient as well as the fatigue calculations for the finite differences can be done in parallel for each material point.

The numerical optimization results show that our original approach supports all stress-based damage parameter types, for example, Brown–Miller, Normal Stress, von Mises, Signed Von Mises, etc. Typically, previous works support only a single damage parameter type. Each extension of the previous reported workflows for supporting additional damage parameters requires new analytical derivations and numerical implementations for the adjoint system. Furthermore, the most common industrial standard is the Brown–Miller damage parameter but normally the Brown-Miller damage and, parameter requires critical planes for the fatigue damage calculations. Previous works mainly use von Mises or similar as damage parameter as these do not require critical plane analysis but therefore, do not correctly describe the fatigue damage. Subsequently, a major contribution of the present work is the support of the Brown–Miller damage type in a general setting for semi-analytical adjoint sensitivities that has not been previously shown. The numerical examples also show stable optimization iteration convergences indirectly verifying accurate adjoint sensitivities for the Brown–Miller damage type using critical plane analysis and rainflow counting for the fatigue damage calculation.

Both the theory and the numerical optimization results also show that our semi-analytical adjoint sensitivity approach supports various non-parametric design variable types as shape, bead, and sizing. Additionally, the optimization approach supports common damage sensitivity calculation characteristics such as multiple load cases for nonproportional loading, MSCs, critical plane analysis, and rainflow-counting for all design variable types.

DATA AVAILABILITY STATEMENT

The data that support the findings of this study are available from the corresponding author upon reasonable request.

ACKNOWLEDGMENT

Open Access funding enabled and organized by Projekt DEAL.

ORCID

Roman Sartorti https://orcid.org/0000-0002-3410-8584
Benedikt Kriegesmann https://orcid.org/0000-0001-5330-9886

REFERENCES

1. Miner MA. Cumulative damage in fatigue. *J Appl Mech*. 1945;12:A159-A164. doi:10.1115/1.4009458
2. Amzallag C, Gerey J, Robert J, Bahuaud J. Standardization of the rainflow counting method for fatigue analysis. *Int J Fatigue*. 1994;16:287-293. doi:10.1016/0142-1123(94)90343-3
3. Lee Y, Tjhung T, Jordan A. A life prediction model for welded joints under multiaxial variable amplitude loading histories. *Int J Fatigue*. 2007;29:1162-1173. doi:10.1016/j.ijfatigue.2006.09.014
4. Dong P, Wei Z, Hong JK. A path-dependent cycle counting method for variable-amplitude multi-axial loading. *Int J Fatigue*. 2010;32:720-734. doi:10.1016/j.ijfatigue.2009.10.010
5. Lee Y-L, Barkey ME, Kang H-T. *Metal Fatigue Analysis Handbook*. Butterworth-Heinemann; 2012.
6. Holmberg E, Torstenfelt B, Klarbring A. Stress constrained topology optimization. *Struct Multidiscip Optim*. 2013;48:33-47. doi:10.1007/s00158-012-0880-7
7. Holmberg E, Torstenfelt B, Klarbring A. Fatigue constrained topology optimization. *Struct Multidiscip Optim*. 2014;50:207-219. doi:10.1007/s00158-014-1054-6
8. Jeong SH, Choi D-H, Yoon GH. Fatigue and static failure considerations using a topology optimization method. *Appl Math Model*. 2015;39:1137-1162. doi:10.1016/j.apm.2014.07.020
9. Oest J, Lund E. Topology optimization with finite-life fatigue constraints. *Struct Multidiscip Optim*. 2017;56:1045-1059. doi:10.1007/s00158-017-1701-9
10. Olesen AM, Hermansen SM, Lund E. Simultaneous optimization of topology and print orientation for transversely isotropic fatigue. *Struct Multidiscip Optim*. 2021;64:1041-1062. doi:10.1007/s00158-021-02995-z
11. Zhang S, Le C, Gain AL, Norato JA. Fatigue-based topology optimization with non-proportional loads. *Comput Methods Appl Mech Eng*. 2019;345:805-825. doi:10.1016/j.cma.2018.11.015
12. Suresh S, Lindström SB, Thore C-J, Torstenfelt B, Klarbring A. Topology optimization using a continuous-time high-cycle fatigue model. *Struct Multidiscip Optim*. 2020;61:1011-1025. doi:10.1007/s00158-019-02400-w
13. Suresh S, Lindström SB, Thore C-J, Klarbring A. Topology optimization for transversely isotropic materials with high-cycle fatigue as a constraint. *Struct Multidiscip Optim*. 2021;63:161-172. doi:10.1007/s00158-020-02677-2
14. Oest J, Sørensen R, Overgaard T, Chr L, Lund E. Structural optimization with fatigue and ultimate limit constraints of jacket structures for large offshore wind turbines. *Struct Multidiscip Optim*. 2017;55:779-793. doi:10.1007/s00158-016-1527-x
15. Oest J, Sandal K, Schafhirt S, Stieng LE, Muskulus M. On gradient-based optimization of jacket structures for offshore wind turbines. *Wind Energy*. 2018;21:953-967. doi:10.1002/we.2206
16. Gerzen N, Clausen PM, Suresh S, Pedersen CBW. Fatigue sensitivities for sizing optimization of shell structures. Proceedings of the 12th World Congress on Structural and Multidisciplinary Optimization; 2017:1-13.
17. Zienkiewicz OC, Taylor RL, Fox DD. *The Finite Element Method for Solid and Structural Mechanics*. 6th ed. Butterworth-Heinemann; 2014.
18. Socie D, Marquis G. *Multiaxial Fatigue*. Society of Automotive Engineers; 2000.
19. Dassault Systèmes fe-safe2022. [Online]. www.simulia.com.
20. Brown MW, Miller KJ. A theory for fatigue failure under multiaxial stress-strain conditions. *Proc Inst Mech Eng*. 1973;187:745-755. doi:10.1243/PIME_PROC_1973_187_069_02
21. Draper J. Developing a durability by design process. Proceedings of the ASME International Manufacturing Science and Engineering Conference 2009, MSEC2009; Vol. 1, 2010:311-319. 10.1115/MSEC2009-84064.
22. Nascimento V, Teixeira G. Validation of a numerical procedure for fatigue assessment of a 325mm brake shoe. Proceedings of the 2019 SAE Brasil International Brake and Motion Control Colloquium and Exhibit; 2020. 10.4271/2019-36-0004
23. Meggiolaro MA, de Castro JTP, Wu H. Invariant-based and critical-plane rainflow approaches for fatigue life prediction under multiaxial variable amplitude loading. *Proc Eng*. 2015;101:69-76. doi:10.1016/j.proeng.2015.02.010

24. Bannantine JA. A variable amplitude multiaxial fatigue life prediction method. University of Ilinois at Urbana-Champaign; 1989.
25. Tikri B. A multiaxial variable amplitude fatigue life prediction method based on a plane per plane damage assessment. *Am J Mech Ind Eng*. 2018;3(4):47-54. doi:10.11648/j.ajmie.20180304.12
26. Sigmund O, Maute K. Topology optimization approaches a comparative review. *Struct Multidiscip Optim*. 2013;48:1031-1055. doi:10.1007/s00158-013-0978-6
27. Bletzinger KU, Daoud F, Firl M. Filter techniques in shape optimization with CAD-free parametrization. In: Soares CAM, ed. *III European Conference on Computational Mechanics Solids, Structures and Coupled Problems in Engineering*. Lehrstuhl für Statik, TU München; 2006.
28. Bletzinger KU. A consistent frame for sensitivity filtering and the vertex assigned morphing of optimal shape. *Struct Multidiscip Optim*. 2014;49:873-895. doi:10.1007/s00158-013-1031-5
29. Schmitt O, Steinmann P. Control of minimum member size in parameter-free structural shape optimization by a medial axis approximation. *Comput Mech*. 2018;61:717-727. doi:10.1007/s00466-017-1477-1
30. Kröger J, Rung T. CAD-free hydrodynamic optimisation using consistent kernel-based sensitivity filtering. *Ship Technol Res*. 2016;62:130. doi:10.1080/09377255.2015.1109872
31. Bourdin B. Filters in topology optimization. *Int J Numer Methods Eng*. 2001;50:2143-2158. doi:10.1002/NME.116
32. Bruns TE, Tortorelli DA. Topology optimization of non-linear elastic structures and compliant mechanisms. *Comput Methods Appl Mech Eng*. 2001;190:3443-3459. doi:10.1016/S0045-7825(00)00278-4
33. Tortorelli DA, Michaleris P. Design sensitivity analysis: overview and review. *Inverse Probl Eng*. 1994;1(1):71-105. doi:10.1080/174159794088027573
34. van Keulen F, Haftka RT, Kim NH. Review of options for structural design sensitivity analysis. Part 1: linear systems. *Comput Methods Appl Mech Eng*. 2005;194:3213-3243. doi:10.1016/j.cma.2005.02.002
35. Vidal CA, Haber RB. Design sensitivity analysis for rate-independent elastoplasticity. *Comput Methods Appl Mech Eng*. 1993;107:393-431. doi:10.1016/0045-7825(93)90074-8
36. Michaleris P, Tortorelli DA, Vidal CA. Tangent operators and design sensitivity formulations for transient non-linear coupled problems with applications to elastoplasticity. *Int J Numer Methods Eng*. 1994;37:2471-2499. doi:10.1002/nme.1620371408
37. Le C, Norato J, Bruns T, Ha C, Tortorelli D. Stress-based topology optimization for continua. *Struct Multidiscip Optim*. 2010;41(4):605-620.
38. Dassault Systèmes Tosca2022. [Online]: www.simulia.com.
39. Dassault Systèmes Abaqus2022. [Online]: www.simulia.com.
40. Svanberg K. The method of moving asymptotes—A new method for structural optimization. *Int J Numer Methods Eng*. 1987;24:359-373. doi:10.1002/nme.1620240207
41. Morrow J. Fatigue properties of metals. *Fatigue Design Handbook*. Longmans, Green and Company: Society of Automotive Engineers; 1968:21-30.
42. Goodman J. *Mechanics Applied to Engineering*. 9th ed. Longmans, Green and Company; 1954.
43. Olhoff N. Optimal structural design via bound formulation and mathematical programming. *Discr Methods Struct Optim— Proc Appl*. 1989;42:255-262. doi:10.1007/978-3-642-83707-4_32
44. Taylor JE, Bendsøe MP. An interpretation for min-max structural design problems including a method for relaxing constraints. *Int J Solids Struct*. 1984;20:301-314. doi:10.1016/0020-7683(84)90041-6

How to cite this article: Sartorti R, Möcker T, Kriegesmann B, Pedersen CBW. On non-parametric fatigue optimization. *Int J Numer Methods Eng*. 2022;1-25. doi: 10.1002/nme.7158